Carbon 212 (2023) 118170

Contents lists available at ScienceDirect

Carbon

journal homepage: www.elsevier.com/locate/carbon

In situ nanocompression of carbon black to understand the tribology of contaminated diesel engine oils

A. Al Sheikh Omar [a,*], F. Motamen Salehi [a], M. Bai [b,c], B.J. Inkson [b], A. Morina [a]

[a] University of Leeds, School of Mechanical Engineering, Institute of Functional Surfaces, Leeds, UK
[b] University of Sheffield, Department of Materials Science and Engineering, Sheffield, UK
[c] Centre for Manufacturing and Materials, Coventry University, Coventry, UK

ARTICLE INFO

Keywords:
Soot
In situ SEM
Nanoindentation
Crystal structure
Mechanical properties
Tribology

ABSTRACT

The study has evaluated the role of soot, surrogated by carbon black (CB) experimentally, in affecting the performance of engine oils. It is very well known that the existence of soot in oil produces abrasive wear on contact surfaces. Other mechanisms influence the oil performance such as additives adsorption on soot and oil degradation due to the interactions with soot. Recent research has suggested the existence of another wear mechanism related to soot particles, which remains poorly understood. This study investigates the effect of soot interactions in engine oil on its mechanical properties. Carbon black particles (CBPs) were used in the experiments to simulate real soot in the engine. The microstructure and crystal structure of CBPs compared to real soot were investigated using transmission electron microscopy (TEM) and X-ray diffraction (XRD). *In situ* compression of the single particle was conducted in a scanning electron microscope (SEM) to evaluate the mechanical properties of fresh and aged CBPs with different sizes. The results show that aged CBPs are significantly harder than fresh CBPs, indicating that ageing in oil modifies the turbostratic crystal structure of CBPs and alters its mechanical properties, potentially affecting tribological performance.

1. Introduction

Soot is identified as carbonaceous material (>90% carbon) which is produced during the combustion process in diesel engine [1–3]. Several studies [1–6] have revealed that soot particles typically have a spherical shape with varied sizes from nanometres to aggregates in micrometres. The crystal structure of soot consists of core and shell, which can vary from mostly amorphous or random in the core to the perfectly ordered crystalline structure of graphite in the shell [7]. Based on several studies [8–12], it was proposed that wear on rubbing surfaces is correlated to hard soot particles causing abrasive wear on the surfaces. The change in the crystal structure of soot could influence the wear [1,13–15]. Uy et al. [1] revealed that different types of soot have different crystal structures influencing the hardness of particles and hence wear.

The correlation between the nature of soot and wear is an interesting area in the lubricant industry. Understanding soot particles in terms of structure, morphology and mechanical properties under sliding or compression is a major issue to reduce wear [13,16]. Several studies [13–15,17] have investigated the effect of soot interactions with oils' additives and bulk oil, causing additive adsorption and oil degradation. Salehi et al. [15] studied the absorption of ZDDP additive on soot particles. The authors proposed that additive adsorption on soot particles due to the high reactive surface of soot might cause a change in the mechanical properties of particles. There are complex chemical interactions between the additives themselves and soot in the existence of oxygen at high temperatures [14]. An increase in the soot surface area led to higher interaction between soot particles and additives accelerating the oil degradation [14]. The interaction between calcium phosphates, which is a detergent compound and considered a hard material in nature, and soot particles could change abrasive characteristics of these particles [13]. The effect of soot on oil oxidation has shown that a higher level of soot in engine oil causes a higher oxidation rate [15,17], which could influence the soot microstructure. Soot oxidation occurs when soot particles react with O, O_2 *and* OH. Molecular Oxygen (O_2) plays the main role in this process due to plenty of O_2. The main chemical reactions that contribute to soot oxidation are explained in equations (1)–(3) [18–20]. Several studies [18,21–25] reported the formation of an oxide layer around soot particles due to soot oxidation and oxidation in internal structure of particles [26,27], which could potentially affect mechanical properties of soot particles. Therefore, the

* Corresponding author.
E-mail address: menaals@leeds.ac.uk (A. Al Sheikh Omar).

https://doi.org/10.1016/j.carbon.2023.118170
Received 1 March 2023; Received in revised form 24 May 2023; Accepted 25 May 2023
Available online 2 June 2023

interactions between the additives, oil and soot require more in-depth investigations to understand the exact evolution of the mechanical properties of soot particles using different oil/additive mixtures at same conditions.

$$C_{soot}^{\circ} + O_2 \rightarrow C_{soot-2}H + 2CO \quad (1)$$

$$C_{soot} - H + O \rightarrow C_{soot}^{\circ} + H_2O \quad (2)$$

$$C_{soot}H + OH \rightarrow C_{soot-1}H + CO + H \quad (3)$$

Where; C_{soot}° is dehdrogenated sites on the soot.

The *in situ* TEM nanoindenter technique has been used in several works to identify mechanical properties of nanosize materials such as silicon nanowires [28], silicon nanospheres [29], MoS2 nanoparticles [30], ZnO nanowires [31] and carbon nanotubes [32]. Lahouij et al. [30] studied the mechanical properties of single and agglomerates of soot particles. Sliding and compression tests were performed to investigate the behaviour of soot particles using *in situ* TEM nanoindenter. The results showed that soot in either single or agglomerate state resisted the applied deformation load. The single particle of soot under compression exhibited elastic-plastic behaviour after compression until 7 GPa contact pressure. Jenei et al. [33] performed *in-situ* compression tests in TEM to measure the mechanical properties of soot particles extracted from diesel engine oil. During the compression, soot particles exhibited elastic-plastic behaviour and suffered permanent changes in the size and shape of their structure. The results showed an increase in calculated hardness and Young's modulus of soot particles after consecutive compressions. Up to a contact pressure of 16 GPa was no noticeable fracture observed after compression, while the shape of soot particles was changed. The hardness of soot particles was registered in the range of 3–16 GPa, which is harder than ZDDP tribofilm (2–5 GPa) [33]. Bhowmick et al. [34] performed soot nano-indentation using an atomic force microscope (AFM). The findings demonstrated that a maximum load of 100 μN was recorded to resist the indentation movement into soot particles with no fracture observed. This study, for the first time, will investigate the effect of change in the microstructure of soot on its mechanical properties.

In this study, mechanical properties of CB particles aged in the oil have been measured for the first time using *in situ* compression testing inside SEM. The effect of the change in the crystal structure of CB after being aged on its mechanical properties has been investigated and discussed.

2. Methodology

2.1. Materials and methods

Carbon black particles (CBPs, Monarch120, Cabot Corporation, Massachusetts, USA) were used in this study to simulate soot particles in engine oil. The diameter of a single CBP is less than 50 nm and the particles agglomerate in large clusters. Fully Formulated Oil (FFO) with a viscosity grade of 10W–40 was used in the diesel engine environment. FFO consists of synthetic base oil and several additives including anti-wear additive, dispersant, detergent, and antioxidant additives. The oil containing 1.5 wt% CB has been artificially aged in the lab for 96 h in accordance with ASTM D4636-99 standard [35]. The ageing period is chosen according to the D4636 standard [35], which allows measurable results (e.g. oxidation) to be obtained in a reasonable time [35]. The ageing method was described in detail in our previous papers [14,36].

2.2. Nanoparticles extraction

The CB and real soot particles were extracted from the aged oil and used oil using a centrifuge (Thermo Scientific Heraens, Megafuge 16R) at speed of 12000 rpm for 2 h. To remove the oil from the particles' surfaces after centrifugation, the particles were washed with heptane and centrifuged again as demonstrated in Fig. 1. Finally, the particles were dried in an oven overnight at 40 °C for further analysis.

2.3. In situ SEM nanoindentation

An in-situ nanoindenter system (Alemnis AG, Thun, Switzerland) equipped with a 60° conical diamond tip (tip diameter 0.7 μm, SYNTON-MDP AG, Switzerland) was used inside a FEG-SEM (FEI, Nova NanoSEM 450) for the compression test of a single particle (Fig. 2a and b). The force-displacement curve was recorded together with the SEM imaging of the particle deformation during the indention process. The particles were first dispersed in iso-propanol using an ultrasonic bath for 2 min, and then a droplet was spread on a silicon single-crystal wafer and dried overnight. Nanoparticles were found to stick on the wedge surface by Van der Waals forces (Fig. 3).

Due to restricted time and cost, nanoindentation tests were repeated for aged CBP at size of 210–220 nm as shown in Fig. 4. In addition, nanoindentation tests for fresh and aged CBPs were also tested at two different particles sizes of 130–140 and 210–220 nm. The repeated tests (Fig. 4) reveal remarkably close results of load-displacement curves. Load curve parameters such as deformation load (f_D), maximum load (f_{max}), deformation depth (h_D), final depth (hf) and stiffness ($S = \frac{\Delta f}{\Delta h}$) were obtained from Figure. These parameters are used to understand the change in mechanical properties of CBPs. Table 1 demonstrates load parameters of aged CB at same size. The analysis of load parameters for both tests is approximately close to each other. The maximum load ($f1_{max}$) accompanied with the displacement of 100 nm (Test 1) is higher compared to maximum load ($f2_{max}$) (Table 1) due to higher displacement (105 nm) was applied (Fig. 4).

2.4. Crystal structure analysis

Transmission Electron Microscopy (TEM, FEI Titan Themis Cubed 300) was used in this study to analyse the crystal structure of a small number of CBP/soot nanoparticles at the high spatial resolution, using E-beam energy of 120 keV, with 0.2 eV energy spread.

X-ray Diffraction (XRD, Bruker D8, Germany) was used to identify the crystallographic structure of the crystal structure of CB and soot particles. The scan angle (2θ) ranged between 10 and 90°. The X-ray generator of this technique was 2 KW. Maximum angular speed is 15°/sec. In this study, the two peaks at 2θ positions ~25° and 43° are indexed as the (002) and (100) graphite-type reflections respectively arising from the turbostratic carbon structure [13,37,38].

3. Results

3.1. Physical characterisation of CB and soot

3.1.1. TEM crystal structure

TEM was used to investigate the crystal structure of fresh and aged CB compared to real soot particles. Aged CB and soot particles were extracted from aged oil and used oil respectively by centrifugation. TEM images were captured for 20 different CB clusters (fresh and aged). The crystal structure of primary CB particles (fresh and aged) consists of the inner core and outer shell (Fig. 5a, b, c and d). The shell thickness of as-received CB particles (fresh and aged) is approximately ≤7 nm. The CB shell displays graphene sheets arranged concentrically around the core. The internal structure of CB particles reveals turbostratic domains with randomly oriented graphene platelets. TEM images of aged CB particles show the formation of an additional thin layer outside the shell with a thickness of ≤3 nm (Fig. 5c and d).

A similar layer was found around the outer soot shell in previous studies [18,23]. Some studies [18,22] reported that large particles with a higher degree of crystallinity can block O_2 diffusion through their

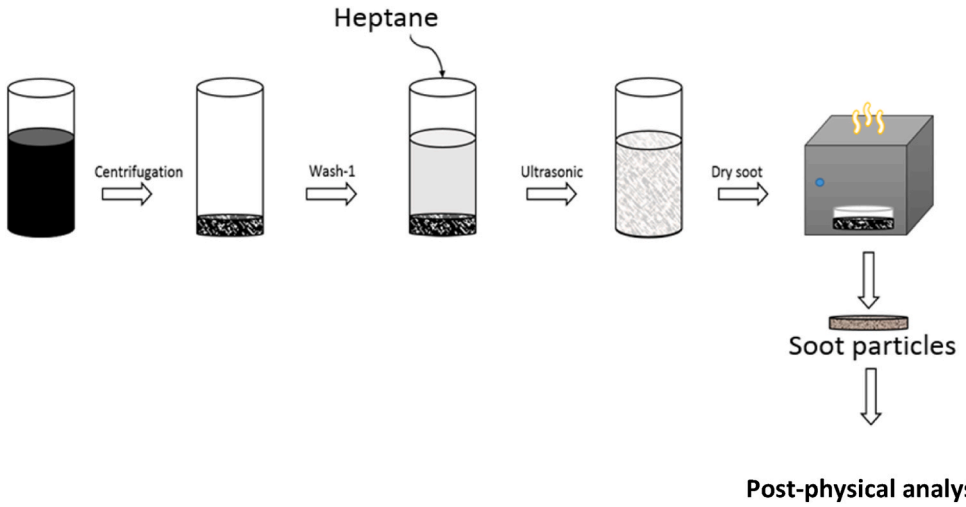

Fig. 1. Diagram of the extraction process of CB/soot particles from the aged oil. (A colour version of this figure can be viewed online.)

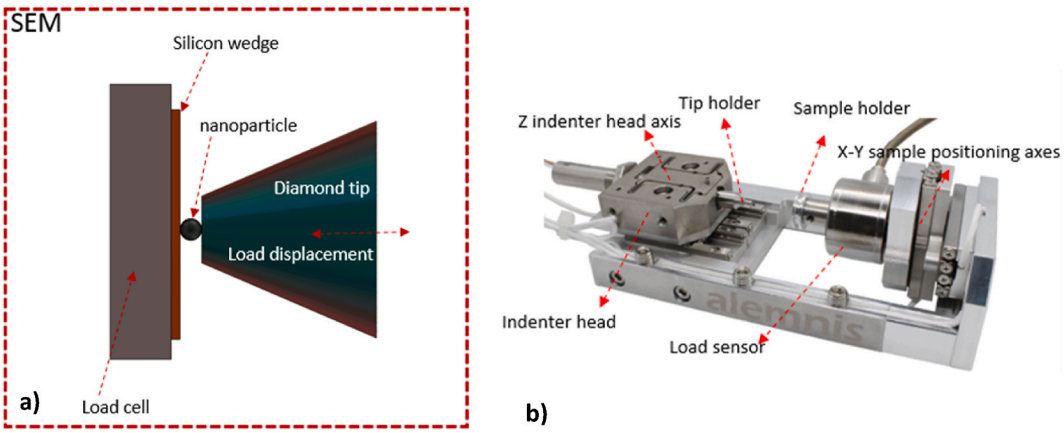

Fig. 2. (a) Schematic representation of nanoindenter performing a compression test on CB particle in the SEM (b) Alemnis nanoindenter. (A colour version of this figure can be viewed online.)

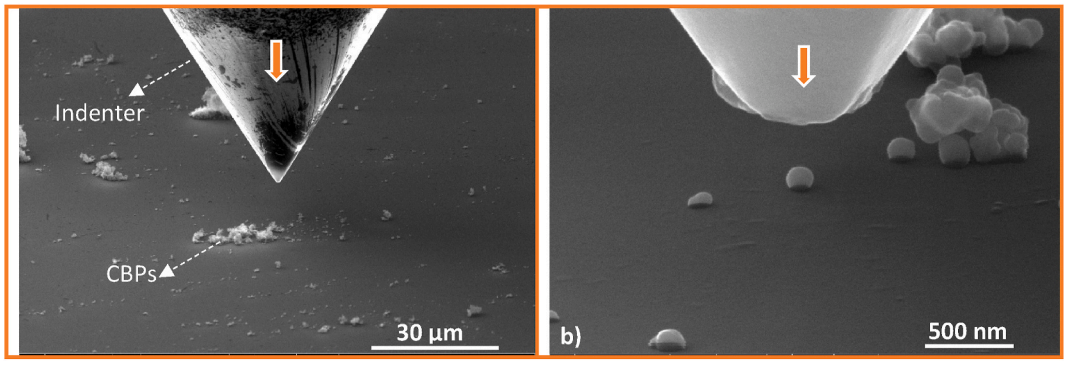

Fig. 3. (a) In situ nanoindentation of CBPs on a Si surface, (b) The diamond indenter is approaching the targeted particle for compressing. (A colour version of this figure can be viewed online.)

outer shell. They proposed that O_2 diffusion into the core is only possible for small particles since for larger particles O_2 atoms react with edge-site atoms of shell particles. The passivated shell does not allow O_2 to access and diffuse through to the reactive amorphous core [18]. This causes the formation of an oxidation layer on the outer shell of aged CB.

The microstructure of the fresh and aged CB particles (Fig. 5) were compared to soot particles extracted from used oil (Fig. 6). The crystal structure of soot consists of core and shell (Fig. 6a and b). TEM images of CB and soot particles show to have similar crystal structure. The graphitic shell thickness of soot subparticles varies and reaches up to 10 nm in some particles as shown in Fig. 6a and b. The soot particles investigated displayed an amorphous layer surrounding the shell with a thickness of less than 2 nm. This thin layer looks similar to the amorphous layer found after ageing CB in the same oil (Fig. 5c and b). This is in line with several studies [18,22,23] reported an amorphous layer surrounded the shell as a result of soot oxidation. The layer surrounding

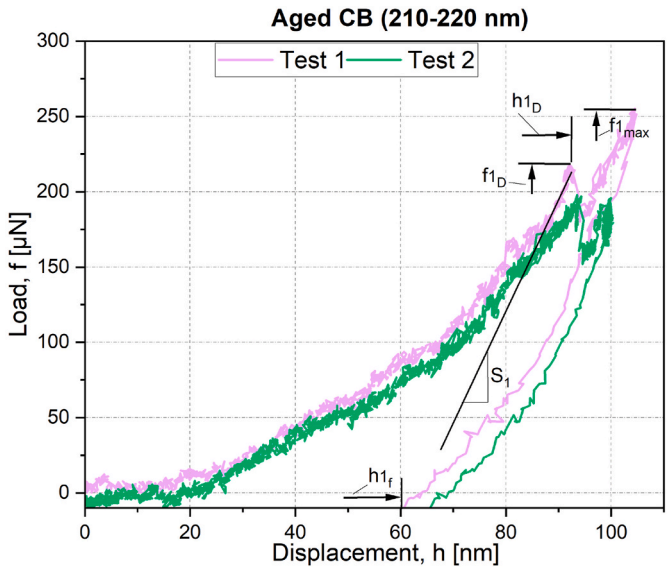

Fig. 4. Load-displacement curves for two repeated nanoindentation tests for aged CBPs that have similar size of (210–220 nm). (A colour version of this figure can be viewed online.)

the soot shell could also contain impurities originating from soot interactions with oil additives at high temperatures. Toth et al. [39] investigated soot oxidation *in situ* and in real-time. The results demonstrated that soot oxidation occurred not only for the particles' surface but also for the internal soot particles that were oxidized.

3.1.2. XRD crystal structure

XRD technique was employed to identify the internal crystalline structure of CB, and the effect of ageing process on the internal structure of CB. TEM results focused on a tiny part of the materials due to the extremely high magnification applied. Thus, the XRD technique was used to get a clear picture of bulk materials, which are usually combinations of many crystallites, particles and other nano-objects. The obtained data about the atomic structure are averaged over the whole sample volume under the probe [37]. In this study, fresh CB, and particles extracted from the oil, including aged CB, and soot particles, were investigated using XRD technique. The XRD information was recorded for the entire scan range of 10–90°θ as shown in Fig. 7.

The X-ray diffraction patterns are composed of two broad peaks at ~25° and 43° (Fig. 7), indexed as the (002) and (100) graphite-type reflections respectively [37,38]. These two peaks are consistent with the turbostratic carbon structure [37,38]. TEM images in this study confirmed the turbostratic structure for CB (fresh and aged) and soot.

XRD result of CB after ageing (Fig. 7b and c) displays a change in peak width (dispersive shoulder peak ranging from 15° to 21.5°). XRD data of aged CB is similar to the study that showed defects of CB atomic [40]. In this study, CB was aged at a high temperature in the presence of additives and oxygen, which influence the CB structure. XRD data of the oxidation of graphite in oils at the same 2θ orientation was investigated by Gupta et al. [41]. The shoulder at 2θ of 15°–21.5° in graphite oxide results [41] is similar to aged CB data in this study. This correlated to the intercalation of oxygen groups that existed in the oil causing oxidation of graphite. Other studies [23,42] found that the existence of oxygen causes soot oxidation for surface particles and the internal structure. In this study, both TEM and XRD results proved the change of CB crystal structure after ageing CB in the oil.

Fig. 7a reveals the crystal structure of soot extracted from the used oil compared to fresh CBP and aged CBP. Similar to fresh and aged CBP analysis, two main peaks at 2θ positions ~25° and 43° are observed in the soot XRD spectrum (Fig. 7a). The small sharp peaks (A, B, C and D) represent various crystalline species, or impurities such as calcium-based compounds, which can also precipitate within oil [2,13]. These peaks (A, B, C and D) indicate that various crystalline species were embedded into turbostratic carbonaceous soot. A similar XRD spectrum of soot analysis (Fig. 7a) was investigated by Sharma et al. [2,13]. XRD data of soot showed a dispersive shoulder peak ranging from ~15°–21.5° which is similar to the aged CB spectrum (Fig. 7b). Dispersive shoulder peak reveals the oxidation of soot particles [41]. The results are in line with TEM images (Fig. 6) that confirmed the change in the crystal structure of CB particles after ageing which is similar to the soot extracted from used oil.

3.2. *In situ* nanoindentation of CBP

3.2.1. Nanocompression of fresh CBP

To evaluate mechanical properties of individual CB particles, *in situ* nanoindentation experiments of fresh CB were performed at two different particle sizes (130–140 nm and 200–240 nm). Fig. 8d demonstrates the recorded load-displacement curve after compressing a 200–240 nm CBP with a diamond tip (Fig. 8a). The CBP particle cracked after approximately 70 nm compressing displacement, at an applied load of 100 μN (called fracture load). The visible surface crack (Fig. 8c) caused a drop in load of 60 μN, but the compressed CBP did not fail completely. Continued indention of the deformed particle and Si substrate increased the applied load to 120 μN. The CB particle under compression undergoes elastic-plastic deformation. In this study, it was difficult to calculate the hardness of particles due to the unknown contact area during compression, however the fracture load can be assessed *in situ*.

In situ nanocompression test was carried out to investigate the deformation of a smaller CB particle with a size of (130–140 nm) (Fig. 9a). The corresponding load-displacement curve reveals deformation in the CB particle after approximately 40 nm compressing displacement corresponding to 20 μN applied load (Fig. 9a). The CB particle after compression is oblate (Fig. 9b). Similar to the (200–240 nm) compression test, the increase in the load after deforming the CBP was correlated to continued indentation into the Si substrate underneath the particle (Fig. 9b). Fig. 9a compares the deformation force to plastically deform the CBP at different sizes (130–140 nm and 200–240 nm). The results show that the larger CBP has higher fracture load compared to the smaller CBP (130–140 nm). The load of the larger particle is 100 μN compared to 25 μN of the smaller CBP.

It is important to note that the compaction of the particles and silicon substrate is partially reversible (Fig. 9a). Lahouij et al. [43] studied nanocompression of soot particles using a TEM nanoindenter. The findings showed that soot particles deform when the contact pressure is above 7 GPa. The soot particles exhibited elastic-plastic behaviour. Bhowmick et al. [34] determined the maximum applied load on soot particles using nanoindentation. The results demonstrated that the maximum applied load on the soot particle is 100 μN before the deformation in the soot particle occurred [34].

Table 1
Load curve parameters for two nanoindentation repeated tests of aged CBPs at size of (210–220 nm) in Fig. 4.

Test details	Deformation load (f_D) (μN)	Max.load (f_{max}) (μN)	Deformation depth (h_D) (nm)	Final depth (h_f) (nm)	Stiffness (S) (μN/nm)
Test 1 **(210–220 nm)**	218	253	92	61	5.4
Test 2 **(210–220 nm)**	199	197	93.5	66	5.8

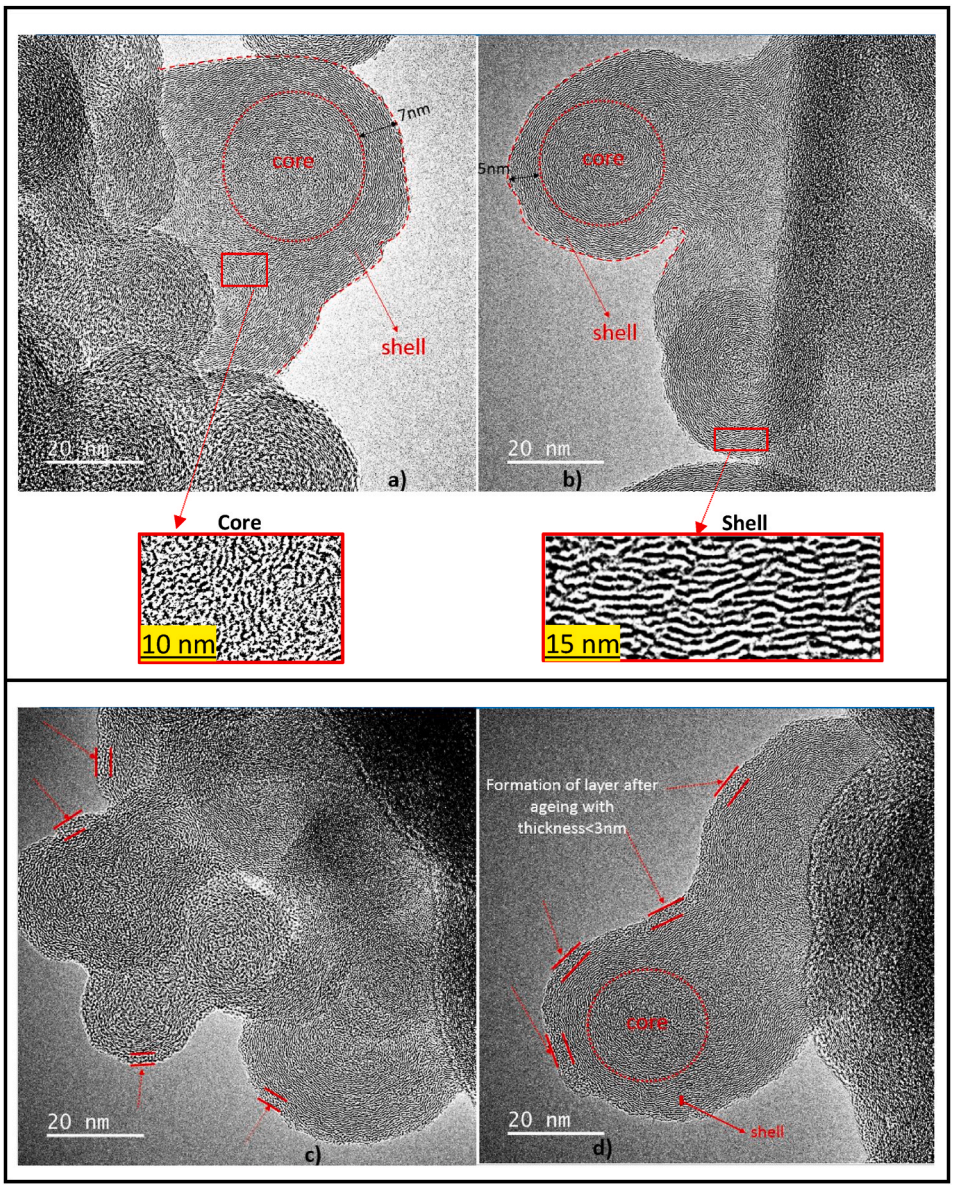

Fig. 5. TEM images of a), b) fresh CB primary particles and c), d) aged CB primary particles. (A colour version of this figure can be viewed online.)

3.2.2. *Nanocompression of aged CBP*

In-situ nanocompression of the aged CBP at different sizes (130–140 nm) and (210–220 nm) were performed to investigate the effect of the ageing process in oil on mechanical properties of CBP. The corresponding load-displacement curve of the 210–220 nm particle is shown in Fig. 10d. During the compression process (Fig. 10b), the applied load increases progressively until particle deformation occurs approximately at 200 μN (90 nm compressing displacement). After the compression test, a surface crack running vertically from the contact zone can be observed in the aged CB particle (Fig. 10c), consistent with the load drop observed.

The load-displacement curves of two different sizes of aged CB particles (130–140 nm) and (210–220 nm) are compared in Fig. 11a. The larger aged-CB particle (210–220 nm) required a higher load to deform the particle compared to the smaller aged-CB particle (130–140 nm). Similar to fresh CB, the larger particle has more resistance to deform compared to smaller CBP, and the observed deformation was the initiation of a radial crack propagating from the indenter contact zone across the CBP surface. The aged-CB particle (130–140 nm) was deformed and oblate after compression as shown in Fig. 11b, and compressed Si substrate underneath the particle (Fig. 11a and b). The fracture load of the larger aged-CB particle is 200 μN compared to 100 μN of the smaller aged-CB particle. The results demonstrate that the aged-CB particle under nanocompression also undergoes elastic-plastic deformation.

The analysis of Load curve parameters for all nanoindentation tests has been conducted in this study are presented in Table 2. The results demonstrated a significant increase in deformation load (f_D) and stiffness (S) after ageing CBPs for two different particles sizes. The increase in maximum load (f_{max}) for aged CBPs is associated with the indentation in Si substrate underneath the tested particle after breaking aged particle, which is higher compared to fresh CBPs. In addition, the deformation depth (h_D) for aged CBPs is higher specifically for larger particle size due to higher load was required to break the particle.

4. Discussion

It has been proposed that the mechanical properties of soot particles are changed in oil at different conditions leading to an increase in wear [34]. Bhowmick et al. [34] and Sharma et al. [13] suggested that chemical interactions between soot and additives could change abrasive

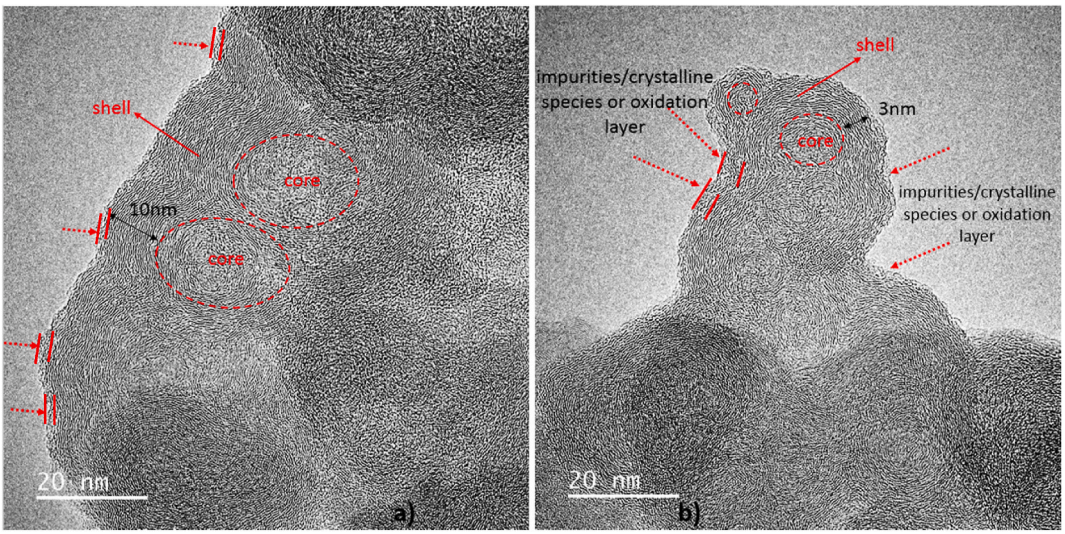

Fig. 6. TEM images (a, b) of the primary soot particles extracted from used oil. (A colour version of this figure can be viewed online.)

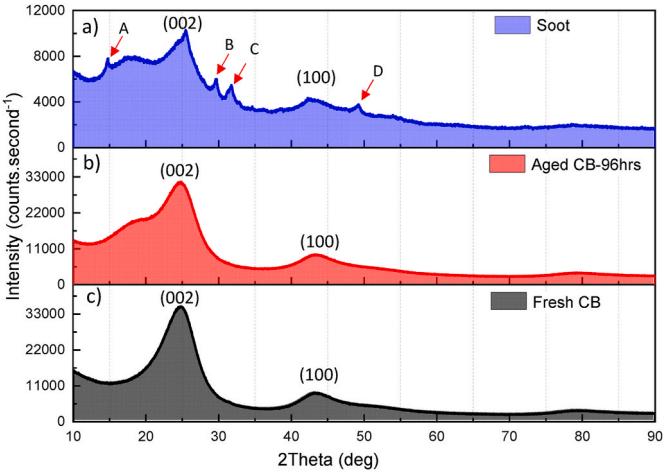

Fig. 7. XRD results of the crystal structure of soot (a), aged CB-96hrs (b) and fresh CB (c). The small sharp peaks A, B, C and D represent various crystalline species or impurities. (A colour version of this figure can be viewed online.)

characteristics of these particles [13]. Our previous study [14] showed the existence of CB in the oil at ageing conditions induced oil oxidation due to the chemical interaction between the CB surface and additives. Other studies [18,22–25,42] reported the formation of an oxidation layer around soot particles and internal soot oxidation which could affect mechanical properties of soot particles. However, there is no evidence to support this hypothesis. This study, for the first time, has investigated the effect of the change in the microstructure of soot on mechanical properties of soot particles.

TEM images (Fig. 5c and d) and XRD data (Fig. 7) revealed that the crystal structure of CB changes after ageing. TEM images (Fig. 5c and d) showed the formation of a layer with a thickness of $\leq$3 nm around aged CB particles. The comparison between the crystal structure of soot and aged CBP demonstrated that the CBP crystal structure is similar to soot. The change in the crystal structure of soot/CB particles after ageing resulted from the oxidation of the soot/CB surface [39,42]. The O_2 diffuses through the outer shell of the particles to react with edge-site atoms of shell particles. The passivated shell did not allow O_2 to access and diffuse through the reactive amorphous core forming the oxidation layer on the outer shell of CB or soot [22,24,25]. The results are in line with other studies that demonstrated the formation of the oxidation layer around soot particles [18,22–25,42]. While other studies [17,39,42] found that internal soot particles were also oxidized causing the change in the microstructure of soot.

The *in situ* SEM nanoindentation of CB revealed that the applied load required to initiate significant plastic deformation of CB after ageing increased significantly for particles in two different sizes (Fig. 12). The increase in the deformation load correlates with a higher particle hardness, meaning a higher compressive load is required to deform/break the CB particles after ageing in the oil. The hardness of the CB is increased due to the change in the crystal structure of CB particles after ageing. A higher deformation load was required to deform the larger particle for both aged and fresh CB.

The results are in the line with other studies [1,13,34] that proposed the change in mechanical properties of soot after ageing. This is the first study that has investigated the relationship between the change in the crystal structure of CB after ageing in the oil and mechanical properties of CB. These findings are in line with Uy et al. [1] who showed that different types of soot, extracted from various oils, had different morphology which could affect the hardness of particles and hence the wear. The findings in this study support other studies [8–12] proposed that changes in the crystal of soot particles due to interactions with additives influence mechanical properties of soot and hence wear [13–15].

5. Conclusions

In this study, the change in mechanical properties of CBPs after interactions in engine oil under ageing conditions has been investigated. It has previously been reported that soot/CB can adsorb oil additives and induce oil degradation which influence wear. However, no experimental studies have addressed the effect of additives interactions with soot/CBPs on its microstructure which could influence mechanical properties of particles becoming harder. The following conclusions are summarised:

- The microstructure of CBP after ageing in engine oil was changed with the formation of a thin amorphous layer around the particles.
- In general, CB particles before and after ageing exhibited size dependent elastic-plastic deformation under nanocompression tests. Larger CBPs exhibited surface cracking.
- For a given particle size, nano-compression experiments revealed that the load required to deform/crack the CBP after oil ageing was approximately double compared to that for pristine CBP, indicating substantial hardening.

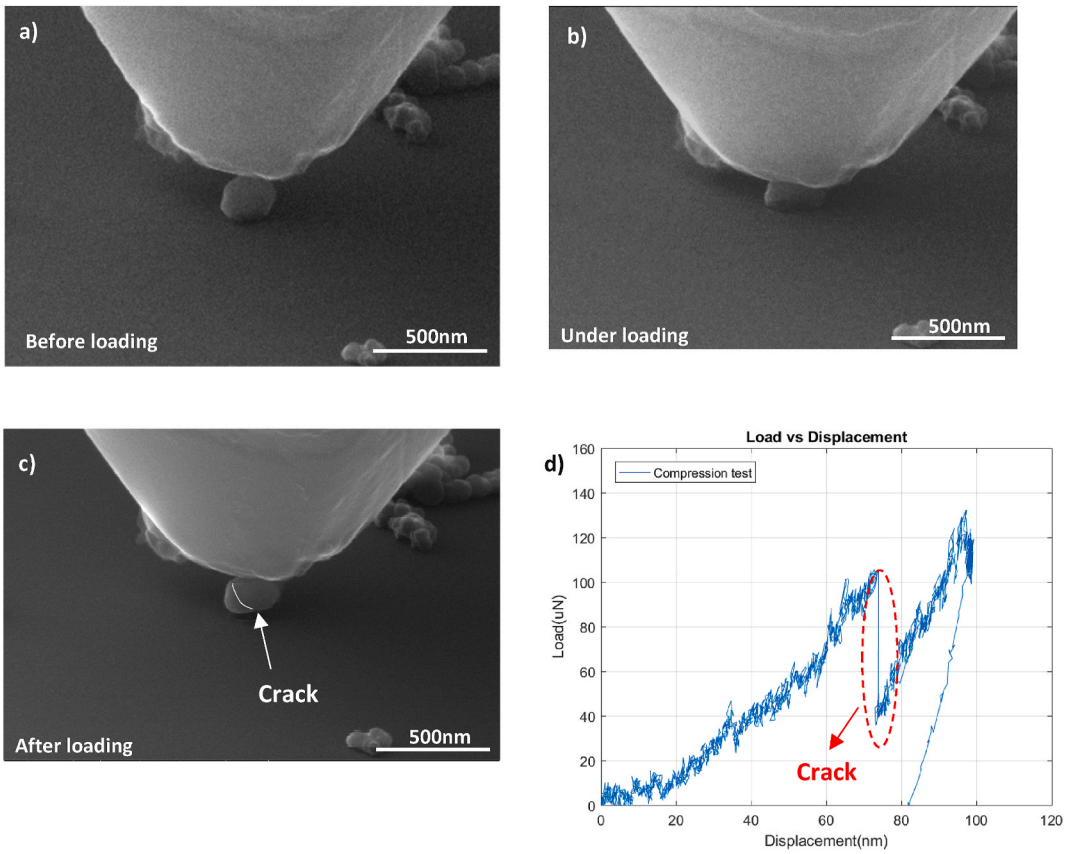

Fig. 8. Nanocompression test of fresh CB particle of size 200–240 nm (a) before loading, (b) under loading, (c) after loading, (d) load-displacement curve. (A colour version of this figure can be viewed online.)

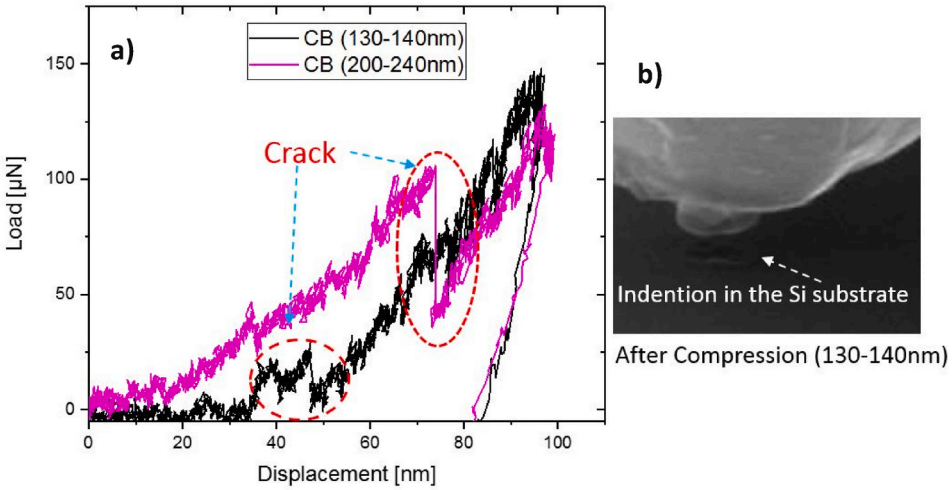

Fig. 9. (a) Nanocompression tests of fresh CBP by diamond at different sizes, (b) Residual indention in Si substrate after compressing a (130–140 nm) particle. (A colour version of this figure can be viewed online.)

- The findings established for the first time that the change in CB microstructure due to chemical interactions with additives causing a change in mechanical properties of CBP. Further repeatability of nanocompression tests with different particles sizes and conditions will enrich these findings.

CRediT authorship contribution statement

A. Al Sheikh Omar: Methodology, Formal analysis, Writing – organal draft, Writing – review & editing. **F. Motamen Salehi:** Supervision, Writing - review & editing. **M. Bai:** Writing – review & editing. **B. J. Inkson:** Writing – review & editing. **A. Morina:** Supervision, Writing - review & editing.

Declaration of competing interest

The authors declare that they have no known competing financial interests or personal relationships that could have appeared to influence

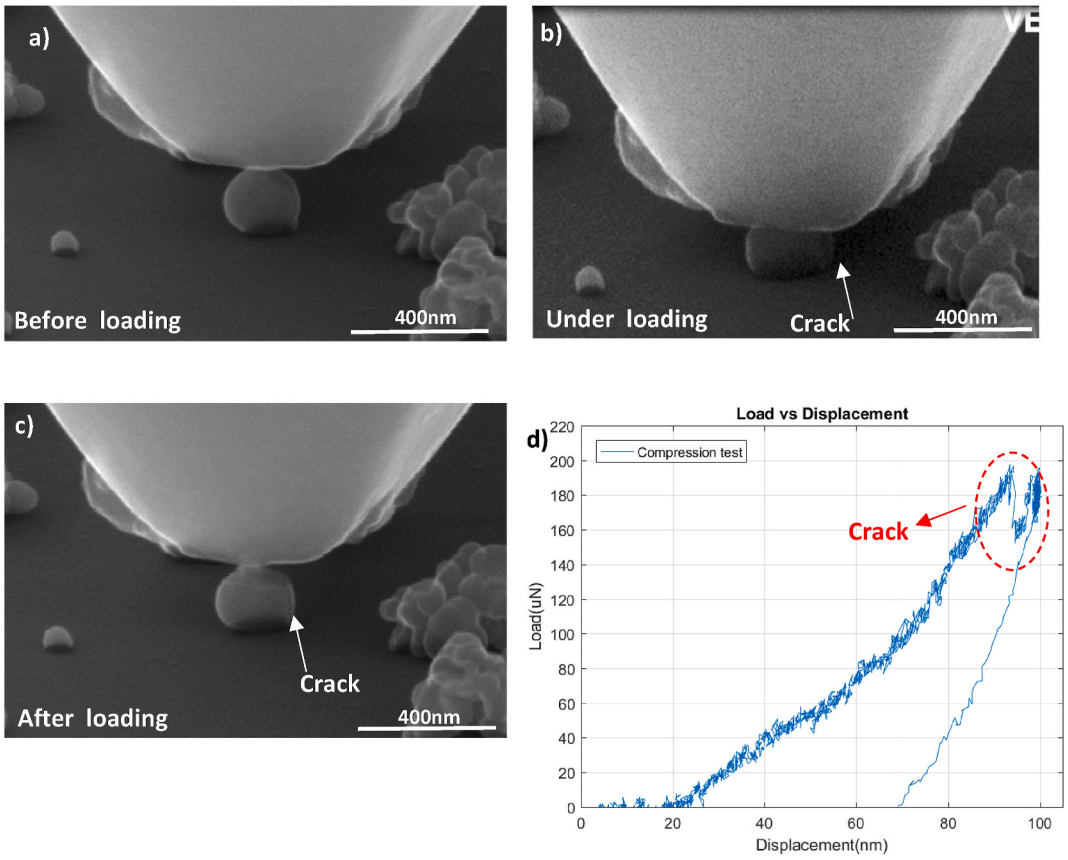

Fig. 10. Nano-compression test aged CBP at size (210–220 nm) (a) before loading, (b) under loading, (c) after loading, (d) load-displacement curve. (A colour version of this figure can be viewed online.)

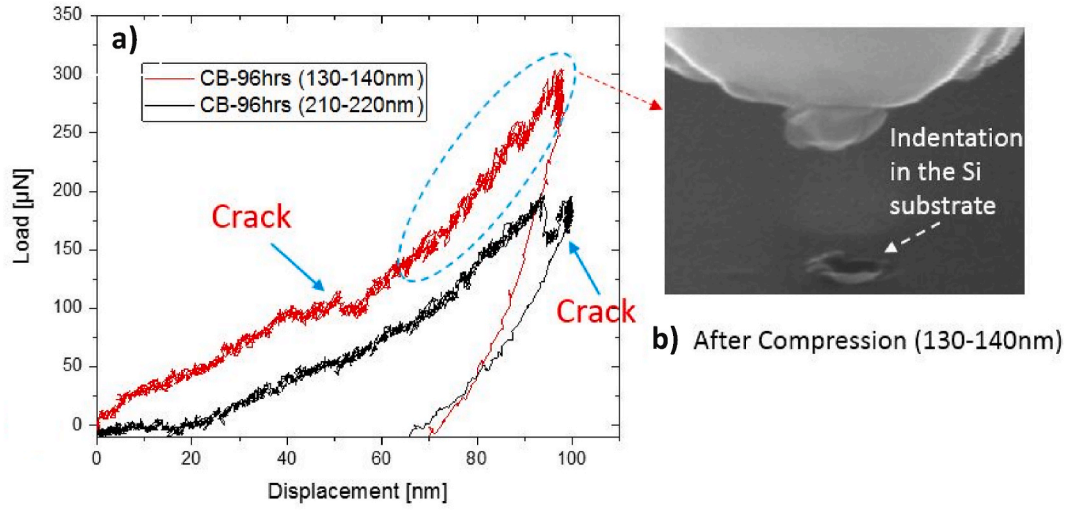

Fig. 11. Nanocompression tests of aged CBP at different sizes, b) indention in the Si substrate after compressing 130–140 nm particle. (A colour version of this figure can be viewed online.)

Table 2
Load curve parameters for fresh and aged CBPs at size of (130–140 nm) and (210–220 nm) which are obtained from load-displacement curves for each test.

Test details	Deformation load (f_D) (μN)	Max.load (f_{max}) (μN)	Deformation depth (h_D) (nm)	Final depth (h_f) (nm)	Stiffness (S) (μN/nm)
Fresh CB **(130–140 nm)**	22.4	148	38.7	83	3.5
Aged CB **(130–140 nm)**	96	303	41	70	5.3
Fresh CB **(210–220 nm)**	105	132	73	82	3.2
Aged CB **(210–220 nm)**	199	197	93.5	66	5.4

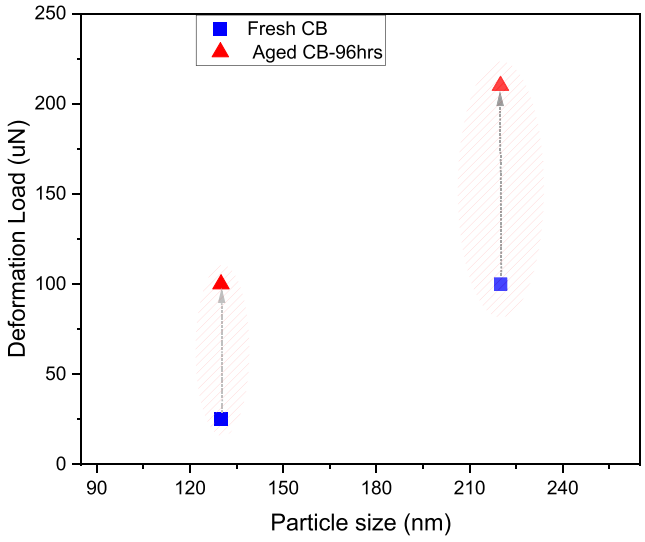

Fig. 12. Deformation load (f_D) of CB after ageing in oil for two different sizes. The deformation load was measured *in situ* at the point where the CB particles were deformed/cracked during nano-compression tests. (A colour version of this figure can be viewed online.)

the work reported in this paper.

Acknowledgements

The authors would like to thank Parker Hannifin Ltd and the EPSRC Centre for Doctoral Training for Integrated Tribology for providing the fund for this research. Grant No. EP/l01629X/1. This work is supported by the Engineering and Physical Sciences Research Council (Grant number EP/R001766/1) as a part of 'Friction: The Tribology Enigma' (www.friction.org.uk), a collaborative Programme Grant between the Universities of Leeds and Sheffield.

The authors would like to pay their gratitude and respects to Professor Anne Neville who passed away in July of 2022. Anne contributed to establishing the research programme presented in this paper.

References

[1] D. Uy, et al., Characterization of gasoline soot and comparison to diesel soot: morphology, chemistry, and wear, Tribol. Int. 80 (2014) 198–209, https://doi.org/10.1016/j.triboint.2014.06.009.
[2] V. Sharma, et al., Structure and chemistry of crankcase and exhaust soot extracted from diesel engines, Carbon N Y 103 (Jul. 2016) 327–338, https://doi.org/10.1016/j.carbon.2016.03.024.
[3] M. Patel, C.L. Azanza Ricardo, P. Scardi, P.B. Aswath, Morphology, structure and chemistry of extracted diesel soot - Part I: transmission electron microscopy, Raman spectroscopy, X-ray photoelectron spectroscopy and synchrotron X-ray diffraction study, Tribol. Int. 52 (Aug. 2012) 29–39, https://doi.org/10.1016/j.triboint.2012.03.004.
[4] V. Sharma, et al., Structure and chemistry of crankcase and exhaust soot extracted from diesel engines, Carbon N Y 103 (Jul. 2016) 327–338, https://doi.org/10.1016/j.carbon.2016.03.024.
[5] A. La Rocca, G. Di Liberto, P.J. Shayler, C.D.J. Parmenter, M.W. Fay, Application of nanoparticle tracking analysis platform for the measurement of soot-in-oil agglomerates from automotive engines, Tribol. Int. 70 (2014) 142–147, https://doi.org/10.1016/j.triboint.2013.09.018.
[6] A. La Rocca, G. Di Liberto, P.J. Shayler, M.W. Fay, The nanostructure of soot-in-oil particles and agglomerates from an automotive diesel engine, Tribol. Int. 61 (2013) 80–87, https://doi.org/10.1016/j.triboint.2012.12.002.
[7] H. Bhowmick, S.K. Biswas, Relationship between physical structure and tribology of single soot particles generated by burning ethylene, Tribol. Lett. 44 (2) (Nov. 2011) 139–149, https://doi.org/10.1007/s11249-011-9831-5.
[8] C.C. Kuo, C.A. Passut, T. Chi Jao, A.A. Csontos, J.M. Howe, Wear mechanism in cummins M-11 high soot diesel test engines, SAE Trans. 107 (1998) 499–511.
[9] D.A. Green, R. Lewis, R.S. Dwyer-Joyce, Wear effects and mechanisms of soot-contaminated automotive lubricants, in: Proceedings of the Institution of Mechanical Engineers, Part J: Journal of Engineering Tribology, 2006, pp. 159–169, https://doi.org/10.1243/13506501JET140.
[10] F. Chinās-Castillo and H. A. Spikes, 'The Behavior of Diluted Sooted Oils in Lubricated Contacts'.
[11] D.A. Green, R. Lewis, The effects of soot-contaminated engine oil on wear and friction: a review, Proc. Inst. Mech. Eng. - Part D J. Automob. Eng. 222 (9) (Sep. 2008) 1669–1689, https://doi.org/10.1243/09544070JAUTO468.
[12] Y. Gallo, et al., Investigation of late-cycle soot oxidation using laser extinction and in-cylinder gas sampling at varying inlet oxygen concentrations in diesel engines, Fuel 193 (2017) 308–314, https://doi.org/10.1016/j.fuel.2016.12.013.
[13] V. Sharma, S. Bagi, M. Patel, O. Aderniran, P.B. Aswath, Influence of engine age on morphology and chemistry of diesel soot extracted from crankcase oil, Energy Fuel. 30 (3) (Mar. 2016) 2276–2284, https://doi.org/10.1021/acs.energyfuels.5b02512.
[14] A. Al Sheikh Omar, F. Motamen Salehi, U. Farooq, A. Morina, A. Neville, Chemical and physical assessment of engine oils degradation and additive depletion by soot, Tribol. Int. 160 (2021), https://doi.org/10.1016/j.triboint.2021.107054.
[15] F. Motamen Salehi, A. Morina, A. Neville, Zinc dialkyldithiophosphate additive adsorption on carbon black particles, Tribol. Lett. 66 (3) (Sep. 2018), https://doi.org/10.1007/s11249-018-1070-6.
[16] H. Bhowmick, S.K. Biswas, Relationship between physical structure and tribology of single soot particles generated by burning ethylene, Tribol. Lett. 44 (2) (Nov. 2011) 139–149, https://doi.org/10.1007/s11249-011-9831-5.
[17] R. Penchaliah, T.J. Harvey, R.J.K. Wood, K. Nelson, H.E.G. Powrie, The effects of diesel contaminants on tribological performance on sliding steel on steel contacts, in: Proceedings of the Institution of Mechanical Engineers, Part J: Journal of Engineering Tribology, Aug. 2011, pp. 779–797, https://doi.org/10.1177/1350650111409825.
[18] H. Ghiassi, I.C. Jaramillo, P. Toth, J.A.S. Lighty, Soot oxidation-induced fragmentation: Part 2: experimental investigation of the mechanism of fragmentation, Combust. Flame 163 (Jan. 2016) 170–178, https://doi.org/10.1016/j.combustflame.2015.09.022.
[19] B.R. Stanmore, J.F. Brilhac, P. Gilot'laboratoire, G. Gilot'laboratoire, The Oxidation of Soot: a Review of Experiments, Mechanisms and Models, 2001.
[20] R. Prasad Neha, S.V. Singh, A review on catalytic oxidation of soot emitted from diesel fuelled engines, J. Environ. Chem. Eng. 8 (4) (Aug. 2020), 103945, https://doi.org/10.1016/J.JECE.2020.103945.
[21] A.Ä. Rpá, B. Palotá, L.C. Rainey, A.F. Sarofim, J.B. Vander Sande, P. Ciambelli, Effect of Oxidation on the Microstructure of Carbon Blacks, 1996 [Online]. Available: https://pubs.acs.org/sharingguidelines.
[22] K. Kamegawa, K. Nishikubo, M. Kodama, Y. Adachi, H. Yoshida, Oxidative Degradation of Carbon Blacks with Nitric Acid II, Formation of water-soluble polynuclear aromatic compounds', 2002.
[23] A.D. Sediako, A. Bennett, W.L. Roberts, M.J. Thomson, In situ imaging studies of combustor pressure effects on soot oxidation, Energy Fuel. 33 (2) (Feb. 2019) 1582–1589, https://doi.org/10.1021/acs.energyfuels.8b03796.
[24] R.H. Hurt, A.F. Sarofim, J.P. Longwell, BRIEF COMMUNICATION Gasification-Induced Densification of Carbons: from Soot to Form Coke, 1993.
[25] J.B. Donnet, J. Schultz, A. Eckhardt, 'ETUDE DE LA MICROSTRUCTURE D'UN NOIR DE CARBONE THERMIQUE', Pergamon Press, 1968.
[26] P. Toth, D. Jacobsson, M. Ek, H. Wiinikka, Real-time, in situ, atomic scale observation of soot oxidation, Carbon N Y 145 (Apr. 2019) 149–160, https://doi.org/10.1016/j.carbon.2019.01.007.
[27] A.D. Sediako, C. Soong, J.Y. Howe, M.R. Kholghy, M.J. Thomson, Real-time observation of soot aggregate oxidation in an environmental transmission electron microscope, Proc. Combust. Inst. 36 (1) (2017) 841–851, https://doi.org/10.1016/j.proci.2016.07.048.
[28] X. Han, K. Zheng, Y. Zhang, X. Zhang, Z. Zhang, Z.L. Wang, Low-temperature in situ large-strain plasticity of silicon nanowires, Adv. Mater. 19 (16) (Aug. 2007) 2112–2118, https://doi.org/10.1002/adma.200602705.
[29] J. Deneen, W.M. Mook, A. Minor, W.W. Gerberich, C.B. Carter, In situ deformation of silicon nanospheres, J. Mater. Sci. (Jul. 2006) 4477–4483, https://doi.org/10.1007/s10853-006-0085-9.
[30] I. Lahouij, F. Dassenoy, B. Vacher, J.M. Martin, Real time TEM imaging of compression and shear of single fullerene-like MoS 2 nanoparticle, Tribol. Lett. 45 (1) (Jan. 2012) 131–141, https://doi.org/10.1007/s11249-011-9873-8.
[31] A. Asthana, K. Momeni, A. Prasad, Y.K. Yap, R.S. Yassar, In situ observation of size-scale effects on the mechanical properties of ZnO nanowires, Nanotechnology 22 (26) (Jul. 2011), https://doi.org/10.1088/0957-4484/22/26/265712.
[32] Z.L. Wang, P. Poncharal, W.A. De Heer, Measuring physical and mechanical properties of individual carbon nanotubes by in situ TEM [Online]. Available: www.elsevier.nl/locate/jpcs.
[33] I.Z. Jenei, et al., Mechanical characterization of diesel soot nanoparticles: in situ compression in a transmission electron microscope and simulations, Nanotechnology 29 (8) (Jan. 2018), https://doi.org/10.1088/1361-6528/aaa2aa.
[34] H. Bhowmick, S.K. Majumdar, S.K. Biswas, Influence of physical structure and chemistry of diesel soot suspended in hexadecane on lubrication of steel-on-steel contact, Wear 300 (1–2) (Mar. 2013) 180–188, https://doi.org/10.1016/j.wear.2013.01.101.
[35] 'Designation: D 4636-99 Standard Test Method for Corrosiveness and Oxidation Stability of Hydraulic Oils, Aircraft Turbine Engine Lubricants, and Other Highly Refined Oils 1'.
[36] A. Al Sheikh Omar, F.M. Salehi, U. Farooq, A. Neville, A. Morina, Effect of zinc dialkyl dithiophosphate replenishment on tribological performance of heavy-duty diesel engine oil, Tribol. Lett. 70 (1) (2022), https://doi.org/10.1007/s11249-022-01565-8.
[37] K. Jurkiewicz, M. Pawlyta, A. Burian, Structure of carbon materials explored by local transmission electron microscopy and global powder diffraction probes, C (Basel) 4 (4) (Dec. 2018) 68, https://doi.org/10.3390/c4040068.

[38] K. Vyavhare, S. Bagi, M. Patel, P.B. Aswath, Impact of diesel engine oil additives-soot interactions on physiochemical, oxidation, and wear characteristics of soot, Energy Fuel. 33 (5) (May 2019) 4515–4530, https://doi.org/10.1021/acs.energyfuels.8b03841.

[39] P. Toth, D. Jacobsson, M. Ek, H. Wiinikka, Real-time, in situ, atomic scale observation of soot oxidation, Carbon N Y 145 (Apr. 2019) 149–160, https://doi.org/10.1016/j.carbon.2019.01.007.

[40] S. Zhang, et al., Control of graphitization degree and defects of carbon blacks through ball-milling, RSC Adv. 4 (1) (2014) 505–509, https://doi.org/10.1039/c3ra44530e.

[41] B. Gupta, N. Kumar, K. Panda, V. Kanan, S. Joshi, I. Visoly-Fisher, Role of oxygen functional groups in reduced graphene oxide for lubrication, Sci. Rep. 7 (Mar. 2017), https://doi.org/10.1038/srep45030.

[42] A.D. Sediako, C. Soong, J.Y. Howe, M.R. Kholghy, M.J. Thomson, Real-time observation of soot aggregate oxidation in an environmental transmission electron microscope, Proc. Combust. Inst. 36 (1) (2017) 841–851, https://doi.org/10.1016/j.proci.2016.07.048.

[43] I. Lahouij, F. Dassenoy, B. Vacher, K. Sinha, D.A. Brass, M. Devine, Understanding the deformation of soot particles/agglomerates in a dynamic contact: tem in situ compression and shear experiments, Tribol. Lett. 53 (1) (Jan. 2014) 91–99, https://doi.org/10.1007/s11249-013-0246-3.